IOP Publishing Measurement Science and Technology

Meas. Sci. Technol. **18** (2007) 2921–2930 doi:10.1088/0957-0233/18/9/023

Automated visual inspection of imprinted pharmaceutical tablets

Marko Bukovec[1,2], Žiga Špiclin[2], Franjo Pernuš[2] and Boštjan Likar[2]

[1] Sensum, Computer Vision Systems, Teslova 30, 1000 Ljubljana, Slovenia
[2] University of Ljubljana, Faculty of Electrical Engineering, Tržaška 25, 1000 Ljubljana, Slovenia

E-mail: marko.bukovec@fe.uni-lj.si, ziga.spiclin@fe.uni-lj.si, franjo.pernus@fe.uni-lj.si and bostjan.likar@fe.uni-lj.si

Received 11 May 2007, in final form 21 June 2007
Published 10 August 2007
Online at stacks.iop.org/MST/18/2921

Abstract

This paper is on automated visual inspection of tablets that may, in contrast to manual tablet sorting, provide objective and reproducible tablet quality assurance. Visual inspection of the ever-increasing numbers of produced imprinted tablets, regulatory enforced for unambiguous identification of active ingredients and dosage strength of each tablet, is especially demanding. The problem becomes more tractable by incorporating some *a priori* knowledge of the imprint shape and/or appearance. For this purpose, we consider two alternative automated tablet defect detection methods. The geometrical method, incorporating geometrical *a priori* knowledge of the imprint shape, enables specific inspection of the imprinted and non-imprinted tablet surface, while the statistical method exploits statistical *a priori* knowledge of tablet surface appearance, derived from a training image database. The two methods were evaluated on a large tablet image database, consisting of 3445 images of four types of imprinted tablets, with and without typical production defects. A 'gold standard' for testing the performances of the two inspection methods was established by manually classifying the tablets into good and five defective classes. The results, obtained by ROC (receiver operating characteristics) analysis, indicate that the statistical method yields better defect detection sensitivity and specificity than the geometrical method. Both presented image analysis methods are quite general and promising tools for automated visual inspection of imprinted pharmaceutical tablets.

Keywords: automated visual inspection, tablets, geometrical models, statistical appearance models, quality control

1. Introduction

Nowadays, pharmaceutical companies produce vast amounts of different tablets worldwide. In the mass production of tablets, various defects can arise during the production processes or even during transportation within production [1]. Visual defects on the tablet surface can have impact on the tablet medication function, tablet identification, the prestige of the manufacturer and on the confidence of the end-user in integrity and quality of the product. For example, the damaged surface of a film-coated tablet accelerates drug release and thereby adversely affects the tablet medication function. On the other hand, clear identification of a tablet by both pharmacists and patients is extremely important in reducing medication error. Therefore, in many countries no tablet may be introduced and commercialized unless it is clearly marked or imprinted with a code imprint that, in conjunction with the tablet's size, shape and colour, permits unique identification of the tablet and the manufacturer. Identification of the tablet requires identification of its active

ingredients and its dosage strength [2]. Imprints are produced by means of embossing, debossing, engraving, or printing with ink. During the production of tablets various surface defects may occur, both in imprint and non-imprint regions, which reduce the overall appearance, quality and identification of the produced tablets. Severe reduction of the readability of imprints by surface defects may result in hazardous mix-ups among various types of tablets possibly endangering patients' health or even life [3]. The manufacturers are obliged and interested in maintaining high quality of tablets from legal, ethical and economical points of view. For example, a whole batch of tablets can be returned to the manufacturer if just a few tablets drastically deviate from the acceptable quality. Furthermore, a patient can have serious doubts and can question the overall medical service if visual quality of a single tablet is low. This is why visual inspection of tablets is of utmost importance for assuring the required quality of different tablets.

Visual inspection of tablets, by which different surface defects are detected, is nowadays predominantly performed manually by various statistical sampling schemes. Such statistical sampling procedures only estimate, at a certain confidence level, the overall quality of a given batch of tablets and can thus not assure the required quality of each tablet. Only if the number of defective tablets in a sample is above a predefined threshold are all tablets in a batch inspected and sorted manually. On the other hand, for more problematic products and demanding markets all tablets in a batch are inspected manually (100% inspection). However, it was reported [4] that manual visual inspection in general, which typically accounts for 10% or more of the total labour cost, can reach only up to 80–90% effectiveness and that human inspectors are prone to reject good products in order to satisfy quotas rather to hold the same quality level. Because manual visual inspection is not only subjective but also slow, unreliable, tedious and even harmful to the operator, only automated visual inspection is nowadays feasible for assuring the required appearance and quality of huge tablet batches.

Automated visual inspection [4, 5] of tablets is very demanding because tablets come in different sizes, shapes, colours and imprints and have different surface defects. Inspection thus requires a sophisticated machine vision system, consisting of fast tablet manipulation, proper illumination, image acquisition and processing, estimation of tablet features/defects and corresponding classification and sorting. There are some companies such as Ackley, Eisai, Ikegami, Mutual, Proditec, Seidenader, Sensum and Viswill that produce and market various automated visual tablet inspection systems. The companies do specify a number of tablet defects that can be detected by their inspection systems but not the corresponding inspection specificities and sensitivities. This is mostly due to the lack of regulation that would enforce generally acceptable testing schemes and thereby enable objective comparison among different inspection systems. While the design of the existing inspection systems is often patented, image analysis algorithms are usually kept confidential but appear to be rather basic because of the demanding real-time inspection requirements (typically 50 or more tablets per second).

An exhaustive search through the literature reveals that although a vast amount of work was done on automated visual inspection of various objects [4, 5], only a few research papers on visual inspection of tablets have been published so far. Deutschl *et al* [6] developed a machine vision system for high speed inspection of a specific type of tablets, i.e. 'extended release tablets', which release their substances at a constant rate over a determined interval through a laser-drilled hole. The inspection goal was to measure the diameter of the laser-drilled hole, which had to be within specified tolerances for proper release of active substances. Dark colour spots and embossed surface defects caused problems in identifying the position of drilled holes. An additional feature was proposed to distinguish holes from surface defects based on monotonically increasing grey values from the darkest point within a potential hole. Silvennoinen *et al* [7] studied the surface and bulk porosities of flat (non-imprinted) tablets with a computer-generated hologram sensor. The pattern of 4×4 laser generated spots was used to investigate a small part of the tablet surface. It was shown for 12 tablets how the specular component of a reflected pattern was related to the tablet surface porosity. Other papers dealt with the effects of mechanical parameter settings on the final tablet structure after compression [8, 9]. Derganc *et al* [10] presented a machine vision system for inspection of non-imprinted tablets in pharmaceutical blisters on a blister-packing machine. The tablets were segmented from the background by a nonparametric MaxShift clustering algorithm. The quality of tablets in blisters was characterized by computing the size, position, shape and surface defects of each segmented tablet. Size and position were computed from the segmented image by component labelling and region boundary extraction, while the tablet shape was assessed by Fourier descriptors. Since only large surface defects with high contrast, which could be segmented from the rest of the tablet surface, were characterized by a single feature, the method proposed by Derganc *et al* [10] addressed mostly the geometrical quality of non-imprinted tablets.

In this paper we consider automated visual inspection of imprinted tablets, before they are packed into blisters or bottles, and focus on various tablet surface defects, which are typically of low contrast and thereby more difficult to detect. The key to reliable tablet surface inspection is the efficient estimation of tablet features, characterizing tablet surface appearance, by means of automated image analysis. Feature estimation is especially demanding when tablets with imprints are inspected as imprinted areas may have significantly different visual properties than the rest of the tablet surface. The problem becomes more manageable if some *a priori* knowledge of the imprint shape and/or appearance is incorporated into the tablet feature estimation. By including prior knowledge, imprinted and non-imprinted tablet regions can be analysed differently and specifically for each tablet type. It is assumed that by partitioning the tablet surface into two non-overlapping constituent regions, each with its specific visual properties, the sensitivity and specificity of the extracted visual features/defects in both tablet regions can be increased.

In this paper, we investigate two alternative methods for tablet specific estimation of appearance features of imprinted tablets. The first method incorporates geometrical *a priori* knowledge of the imprint, which resembles current state of

the art in the field of automated visual inspection of tablets and adds a novel imprint-specific feature. The second method, which incorporates statistical information on the whole tablet appearance, represents our major contribution to the field of automated visual inspection of tablets. The two methods are evaluated on a large image database of imprinted tablets, with and without typical surface defects. Another important contribution of this work is the evaluation methodology that we propose to objectively assess the performances of tablet image analysis methods. The proposed evaluation is based on assessing the sensitivities and specificities for detecting various defects on tablets by the ROC (receiver operating characteristics) analysis. Such a systematic evaluation methodology should form a basis not only for further development and comparison of tablet image analysis methods but also for objectively assessing the performances of the existing and emerging tablet inspection systems.

2. Methods

In this section, the two methods, i.e. the geometrical method that is based on the imprint shape and the statistical method that is based on the statistics of tablet surfaces, are presented. The methods operate on images of tablets and extract different features, which estimate a tablet's surface quality. Features are derived from different column vector representations $\mathbf{x}$ of the tablet image $\mathbf{I}(x, y)$, which are represented in the form of image intensities $\mathbf{i}$, absolute gradients $\mathbf{g}$ and gradient components $\mathbf{c} = \left[\mathbf{c}_x^{\mathrm{T}}, \mathbf{c}_y^{\mathrm{T}}\right]^{\mathrm{T}}$ in the x and y directions.

The segmentation and registration of tablet images are the necessary pre-processing steps of both methods. Segmentation of a tablet surface from the background is performed by the MaxShift clustering algorithm as proposed in [10]. Rigid registration (translation and rotation) of tablet images is needed for bringing tablet imprints into spatial correspondence. The translation parameters are obtained by matching the centre of masses of the segmented tablet surfaces, while the rotation parameter is obtained by matching principal axes [11] of the oblong tablets and by the circular profile matching [12] of the circular tablets.

2.1. Geometrical method

The geometrical method incorporates *a priori* knowledge of the imprint obtained from the geometrical model of the imprint. An example of a T-shaped geometrical imprint model is illustrated in figure 1. The imprint is represented by a skeleton, defining local imprint direction and a binary template of the imprint thickness. Before computing the tablet features, the geometrical model of the imprint is rigidly registered to the image of the analysed tablet.

Five geometrical features are defined to characterize the appearance of a tablet. Four features are computed for the non-imprint regions of a tablet. The first two features are the maximal G_1 and minimal G_2 differences between the original $\mathbf{i}$ and mean filtered $\mathbf{i}^*$ intensities of pixels within $k \in \Omega_1$:

$$G_1 = \max_{k\in\Omega_1}(\mathbf{i}_k - \mathbf{i}_k^*), \qquad G_2 = \min_{k\in\Omega_1}(\mathbf{i}_k - \mathbf{i}_k^*). \tag{1}$$

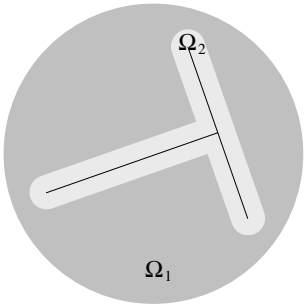

Figure 1. An example of a T-shaped imprint geometrical model, obtained by thickening the skeleton (dark lines). The tablet surface (Ω) is partitioned into non-imprint (Ω_1) and imprint regions (Ω_2).

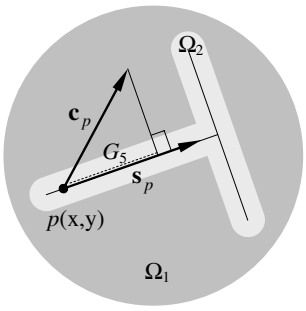

Figure 2. Illustration of the geometrical feature G_5, defined as a scalar product between gradient component $\mathbf{c}_p$ and imprint direction vector $\mathbf{s}_p$ at pixel $p(x, y)$. The G_5 feature, which is represented by the dashed line, is proportional to the component $\mathbf{c}_p$ that is parallel to the $\mathbf{s}_p$ vector.

Subscript k indicates only those elements of intensity vectors $\mathbf{i}$ and $\mathbf{i}^*$ which correspond to the non-imprint area Ω_1.

The next two geometrical features are defined as the maximal G_3 absolute gradient $\mathbf{g}$ and maximal G_4 mean filtered absolute gradient $\mathbf{g}^*$:

$$G_3 = \max_{k\in\Omega_1}\mathbf{g}_k, \qquad G_4 = \max_{k\in\Omega_1}\mathbf{g}_k^*. \tag{2}$$

While the first four geometrical features resemble current state of the art in tablet image analysis, the last geometrical feature G_5 is novel and imprint specific. The feature is computed as the maximal norm ($||\cdot||$) of the scalar product ($\cdot$) of the gradient component $\mathbf{c}$ and the normalized local imprint direction vector $\mathbf{s}$, defined by the imprint skeleton

$$G_5 = \max_{p\in\Omega_2}\|\mathbf{c}_p \cdot \mathbf{s}_p\|\|\mathbf{s}_p\|^{-1}, \tag{3}$$

where $\mathbf{c}_p$ and $\mathbf{s}_p$ respectively represent the gradient component vector $\mathbf{c}$ and normalized local imprint direction vector $\mathbf{s}$ at each image point $p(x, y)$ (figure 2):

$$\mathbf{c}_p = [c_x \;\; c_y]^{\mathrm{T}} \qquad \text{and} \qquad \mathbf{s}_p = [s_x \;\; s_y]^{\mathrm{T}}. \tag{4}$$

Direction of the vector $\mathbf{s}_p$ in the imprint region where two or more skeleton areas overlap is defined by the direction of the closest skeleton segment.

2.2. Statistical method

The statistical method exploits the *a priori* knowledge in the form of a statistical appearance model of a tablet. The

statistical appearance model is first derived from rigidly registered images of a training image database and then registered to the image of the analysed tablet. In this way, not only the imprint and non-imprint tablet regions but also each image element (pixel) is inherently analysed distinctively and specifically for each tablet type.

Principal component analysis [13, 14] is used to statistically model the tablet appearance $\mathbf{x}$ by a linear model:

$$\mathbf{x} = \bar{\mathbf{x}} + \mathbf{A}\mathbf{p}, \tag{5}$$

consisting of the average appearance $\bar{\mathbf{x}}$ and a linear combination of principal components $\mathbf{A}$ of appearances with corresponding parameters $\mathbf{p}$. To obtain a linear model, the N aligned training images $\mathbf{I}_1 \ldots \mathbf{I}_N$ are converted to column vector representations $\mathbf{x}_1 \ldots \mathbf{x}_N$ and the corresponding average column vector $\bar{\mathbf{x}}$ and covariance matrix $\boldsymbol{\Theta}$ are computed:

$$\boldsymbol{\Theta} = E((\mathbf{x} - \bar{\mathbf{x}})(\mathbf{x} - \bar{\mathbf{x}})^{\mathrm{T}}). \tag{6}$$

Next, the eigenvalues and corresponding eigenvectors of the covariance matrix $\boldsymbol{\Theta}$ are obtained by singular value decomposition [15]. The eigenvectors of the largest eigenvalues represent the most significant modes of variation of tablet appearance over a set of training images. Tablet appearance can thus be approximated by only the first t most significant eigenvectors:

$$\mathbf{x} \approx \tilde{\mathbf{x}} = \bar{\mathbf{x}} + \mathbf{A}_t \mathbf{p}_t, \tag{7}$$

where $\tilde{\mathbf{x}}$ denotes an approximation of $\mathbf{x}$, $\mathbf{A}_t$ the first t eigenvectors of $\boldsymbol{\Theta}$ and $\boldsymbol{p}_t$ a vector of t appearance approximation parameters, i.e. projections of $(\mathbf{x} - \bar{\mathbf{x}})$ to the corresponding t eigenvectors. In this way, a compact statistical model, representing *a priori* knowledge of tablet appearance, can be obtained for any tablet image representation $\mathbf{x}$. In our case, we have used image intensities $\mathbf{i}$, absolute gradients $\mathbf{g}$ and gradient components $\mathbf{c}$ of the tablet images and derived the corresponding statistical models of their appearances. The obtained statistical models are used to derive various so-called statistical features of tablet images aligned with the statistical models.

The first statistical feature is the maximal absolute ($|\cdot|$) difference S_1 between the tablet image intensity representation $\mathbf{i}$ and the corresponding statistical model $\tilde{\mathbf{i}}$, over the entire tablet surface domain $k \in \Omega$:

$$S_1 = \max_{k \in \Omega} |\mathbf{i}_k - \tilde{\mathbf{i}}_k|. \tag{8}$$

The second statistical feature is the maximal absolute difference S_2 between the tablet image gradient representation $\mathbf{g}$ and corresponding statistical model $\tilde{\mathbf{g}}$, over the entire tablet surface domain $k \in \Omega$:

$$S_2 = \max_{k \in \Omega} |\mathbf{g}_k - \tilde{\mathbf{g}}_k|. \tag{9}$$

The last three statistical features are obtained from the gradient components $\mathbf{c}$ of the analysed tablet images and the corresponding statistical model $\tilde{\mathbf{c}}$ (figure 3) as the maximal norm of a vector difference S_3:

$$S_3 = \max_{p \in \Omega} \|\mathbf{c}_p - \tilde{\mathbf{c}}_p\|, \tag{10}$$

a vector product S_4:

$$S_4 = \max_{p \in \Omega} \|\mathbf{c}_p \times \tilde{\mathbf{c}}_p\|, \tag{11}$$

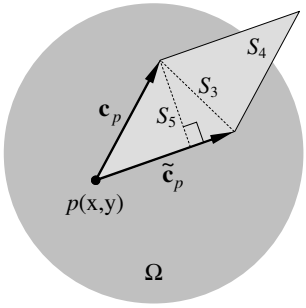

Figure 3. Illustration of the three statistical features S_3–S_5 obtained from the gradient component $\mathbf{c}_p$ and the corresponding statistical model $\tilde{\mathbf{c}}_p$ at point $p(x, y)$. Features S_3 and S_5 are represented by two dashed lines, while S_4 is illustrated by the area of a parallelogram spanned over the two vectors.

and a normalized vector product S_5:

$$S_5 = \max_{p \in \Omega} \|\mathbf{c}_p \times \tilde{\mathbf{c}}_p\| \|\tilde{\mathbf{c}}_p\|^{-1}, \tag{12}$$

where $\mathbf{c}_p$ and $\tilde{\mathbf{c}}_p$ respectively denote the values of gradient components of an inspected tablet and the corresponding statistical model at each image point $p(x, y) \in \Omega$:

$$\mathbf{c}_p = [c_x \;\; c_y]^{\mathrm{T}} \qquad \text{and} \qquad \tilde{\mathbf{c}}_p = [\tilde{c}_x \;\; \tilde{c}_y]^{\mathrm{T}}. \tag{13}$$

3. Experiments and results

In this section, implementation details, the experimental tablet image database with the 'gold standard' and the evaluation methodology are presented first. Next, the defect detection results obtained by the five geometrical and five statistical features are given.

3.1. Implementation details

Filtered image intensities $\mathbf{i}^*$, absolute gradients $\mathbf{g}$ and gradient components $\mathbf{c}$ were obtained from the original grey-scale intensities $\mathbf{i}$ using a mean filter with a 5×5 kernel, while a 20×20 kernel was used for filtering the absolute gradients $\mathbf{g}^*$. Image gradients were approximated by symmetric differences of filtered image intensities [16]. The statistical models of appearances of each tablet type were derived from 80 training images of non-defective tablets and approximated by the first three eigenvectors ($t = 3$).

3.2. Image database with 'gold standard'

The experimental image database consisted of 3445 images of four types of imprinted tablets in sets of 830, 1208, 821 and 586 tablets, with and without typical production defects (figure 4). All four tablet types have debossed imprints, i.e. imprints below the tablet surface. The first two tablet types have similar line-shaped imprints and an almost flat tablet surface, while the imprint cross-section profiles were slightly different. Tablets in the third and fourth sets have a convex tablet surface and imprints with the text '500' and 'RTD75', respectively.

Tablet images were captured by a Sensum SPINE machine vision system (www.sensum.eu), consisting of a trilinear line-scan camera and white LED illumination directed from a

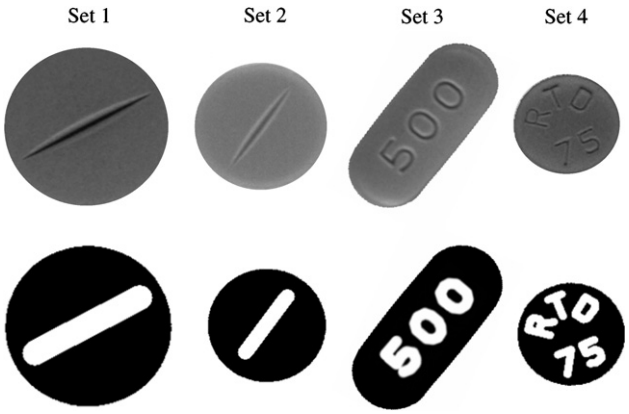

Figure 4. Four tablet types from left to right (top) with the corresponding imprint regions (bottom).

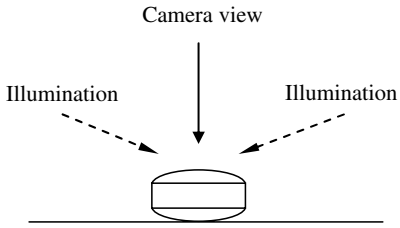

Figure 5. Experimental setup scheme.

low angle to the tablet surface (figure 5). Such a low angle illumination enhances the contrast on both tablet imprints and surface defects that rise above and below the tablet surface.

A 'gold standard' for visual inspection of defects was established by carefully manually classifying the tablets as non-defective and defective ones, which were further classified into five defect categories, named: 'dot' (D_1), 'spot' (D_2), 'emboss' (D_3), 'deboss' (D_4) and 'crack' (D_5), as illustrated by the examples in figure 6.

3.3. Evaluation methodology

The specificities and corresponding sensitivities of geometrical (G_1–G_5) and statistical (S_1–S_5) features for each defect category and for each tablet set were obtained by the receiver operating characteristics (ROC) analysis [17]. The ROC curve relates the tradeoffs between the true positive (TPR) and the corresponding false positive (FPR) defect detection rate of each feature (figure 7). The TPR = TP/P is the ratio between the number of correctly detected tablets with defects (TP) and all defective (P) tablets (see figure 7, top left), while the FPR = FP/N represents the ratio between the number of incorrectly detected non-defective tablets (FP) and all non-defective (N) tablets (see figure 7, top left). TPR is a measure of sensitivity, while 1 − FPR is a measure of defect detection specificity. A ROC curve is insensitive to the ratio between the number of defective (P) and non-defective (N) 'gold standard' samples used for evaluation [17].

Two quantitative evaluation criteria $\mathrm{TPR_{FPR}}$ and $\mathrm{AUC_{FPR}}$ were derived from the ROC curves. The $\mathrm{TPR_{FPR}}$, which is defined as the value of TPR at a given FPR, represents the ratio of correctly detected defective tablets at a given ratio of incorrectly detected good tablets (figure 7). The $\mathrm{AUC_{FPR}}$ is defined as the area under the ROC curve from 0 to a given FPR, normalized by FPR:

$$\mathrm{AUC_{FPR}} = \frac{1}{\mathrm{FPR}} \int_0^{\mathrm{FPR}} \mathrm{TPR}_x \, \mathrm{d}x. \tag{14}$$

$\mathrm{AUC_{FPR}}$ estimates the average defect detection performance over a practically acceptable FPR value (figure 7). FPR was set to 0.1 and corresponding $\mathrm{TPR_{0.1}}$ and $\mathrm{AUC_{0.1}}$ were computed from the ROC curves of all geometrical and statistical features and all defect categories. Besides, for each feature its defect detection potential was defined as the total area ($\mathrm{AUC_1}$) under a corresponding ROC curve. To assess both the defect-specific and general defect detection potential of individual features, $\mathrm{AUC_1}$ values were calculated for individual defect categories and the obtained values were then summarized over all defects. Finally, the detection of all defects ($D_{1–5}$) by the joined geometrical ($G_{1–5}$) and statistical ($S_{1–5}$) features was evaluated by computing the AUC values from the ROC curves, which were obtained by linear classification with boundaries parallel to the features axes. Such a classification has some important practical implications. Namely, linear classification with boundaries parallel to the features axes enables independent tuning of individual feature thresholds, inclusion or exclusion of features, requires neither prior knowledge on probability distributions nor classification training, while the operator is kept in a classification loop and has full control over the classification criteria. In this way, appropriate defect inspection sensitivity for various types of tablets

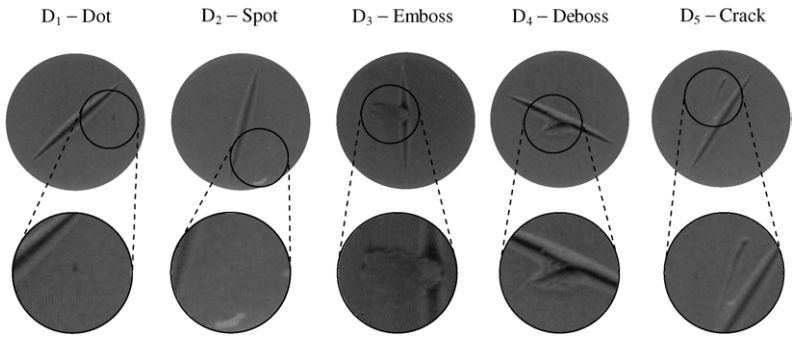

Figure 6. Tablets (top) with zoomed defects (bottom). The images were enhanced in contrast to better visualize the small defects, which would otherwise be hardly visible.

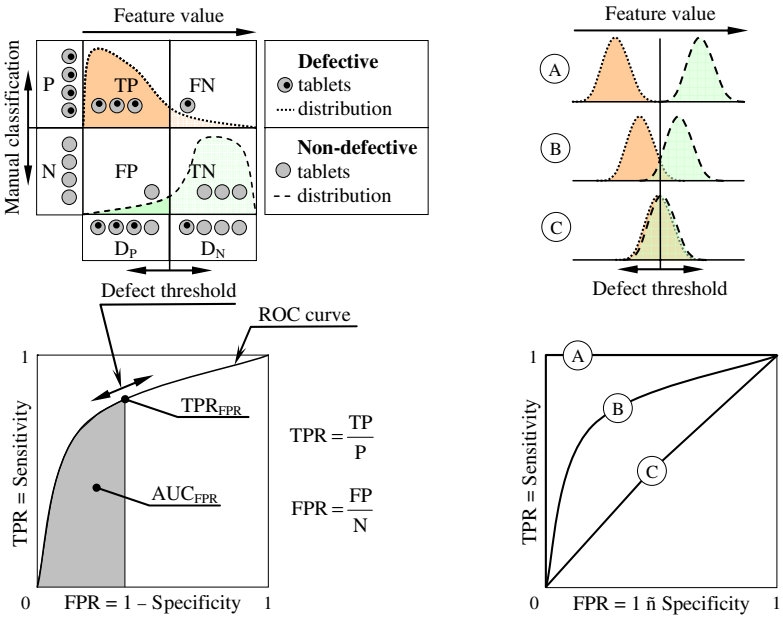

Figure 7. ROC analysis of defect detection sensitivity and specificity and the two evaluation criteria. Left: manually classified 'gold standard' defective (P) and non-defective (N) tablets are generally either detected as defective (D_P) or they are detected as non-defective (D_N) tablets, depending on the frequency distributions and on the selected defect threshold of each feature (top). The TPR_{FPR} and AUC_{FPR} evaluation criteria obtained from a given ROC curve (bottom). Right: distributions of feature values for defective and non-defective products (top) and corresponding ROC curves (bottom): ideal non-overlapping distributions (A), partially overlapping distributions (B) and completely overlapping distributions (C).

Table 1. The $TPR_{0.1}$ and $AUC_{0.1}$ values for all features and five individual defects in the first set of 830 tablet images.

Set 1	D_1		D_2		D_3		D_4		D_5	
Feature	$TPR_{0.1}$	$AUC_{0.1}$	$TPR_{0.1}$	$AUC_{0.1}$	$TPR_{0.1}$	$AUC_{0.1}$	$TPR_{0.1}$	$AUC_{0.1}$	$TPR_{0.1}$	$AUC_{0.1}$
G_1	0.38	0.32	0.57	0.45	0.55	0.53	0.33	0.24	0.76	0.57
G_2	0.70	0.55	0.61	0.55	0.62	0.52	0.37	0.24	0.55	0.44
G_3	0.83	0.73	0.83	0.72	0.58	0.54	0.51	0.44	**1.00**	0.87
G_4	0.90	0.84	**1.00**	**0.98**	0.65	0.57	0.73	0.68	**1.00**	**1.00**
G_5	0.53	0.51	0.36	0.33	0.52	0.30	0.87	0.83	0.05	0.03
S_1	0.94	0.82	0.88	0.75	**1.00**	0.92	**1.00**	0.85	0.95	0.78
S_2	**1.00**	0.91	**1.00**	0.95	**1.00**	0.96	**1.00**	0.92	**1.00**	0.99
S_3	**1.00**	**0.97**	**1.00**	0.97	**1.00**	**1.00**	**1.00**	**1.00**	**1.00**	0.99
S_4	0.64	0.57	0.47	0.39	**1.00**	0.65	0.98	0.92	0.55	0.50
S_5	**1.00**	0.94	**1.00**	0.96	**1.00**	0.93	**1.00**	0.95	**1.00**	0.99

and corresponding tablet specific defects can be selected efficiently. The ROC curve for linear classification with joined features is obtained by a combination of multiple thresholds, each defining a single point on a ROC graph. By varying all individual feature thresholds, a cloud of ROC points is obtained. The ROC curve is defined by a subset of points that yield maximal TPR for each FPR value, i.e. the ROC curve is a convex hull that spans over the cloud of ROC points [17].

3.4. Results

Tables 1 and 2 show the results of defect detection for geometrical and statistical features. In table 1, $TPR_{0.1}$ and $AUC_{0.1}$ values are given for individual defect categories (D_1–D_5) for the first set of tablet images. Table 2 shows the defect detection results for all four tablet types and for all defect categories ($D_{1–5}$). In both tables, the best TPR and AUC values are marked in bold so that the best features for individual defects in each tablet image set can easily be identified.

The obtained results indicate that for all tablet types the statistical feature S_3 performed the best. Besides S_3 the statistical features S_2 and S_5 also performed well on all sets of tablets. The geometrical features, except feature G_4, yielded much lower true positive detection rates on all defects. The comparison of the best geometrical G_4 and the best statistical feature S_3 indicates that S_3 performed much better than G_4. On the first tablet type (table 2) the best geometrical feature G_4 yielded a $TPR_{0.1}$ value of 0.80, while three statistical features performed perfectly with the $TPR_{0.1}$ values of 1. On the second tablet type (table 2) the best geometrical (G_4) and statistical (S_2) features yielded $TPR_{0.1}$ values of 0.67 and 0.91, respectively. On the third and fourth tablet types (table 2) the best geometrical $TPR_{0.1}$ values were 0.94 and 0.59, while the best statistical features yielded $TPR_{0.1}$ values of 0.96 and 0.91, respectively. In the first three tablet image sets the best $AUC_{0.1}$

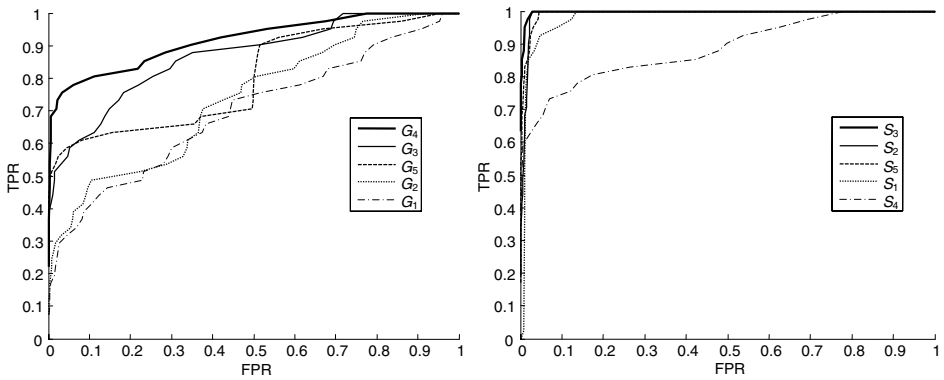

Figure 8. ROC curves of individual geometrical (G_1–G_5, left) and statistical (S_1–S_5, right) features for the first tablet type.

Table 2. The $TPR_{0.1}$ and $AUC_{0.1}$ values for all features and all defect categories ($D_{1–5}$) for all four sets of tablet images.

	Set 1 - $D_{1–5}$		Set 2 - $D_{1–5}$		Set 3 - $D_{1–5}$		Set 4 - $D_{1–5}$	
Feature	$TPR_{0.1}$	$AUC_{0.1}$	$TPR_{0.1}$	$AUC_{0.1}$	$TPR_{0.1}$	$AUC_{0.1}$	$TPR_{0.1}$	$AUC_{0.1}$
G_1	0.41	0.31	0.40	0.30	0.40	0.22	0.23	0.16
G_2	0.47	0.34	0.46	0.32	0.04	0.02	0.26	0.12
G_3	0.63	0.56	0.64	0.51	0.45	0.23	0.59	0.43
G_4	0.80	0.75	0.67	0.55	0.94	0.78	0.41	0.36
G_5	0.62	0.58	0.38	0.32	0.62	0.60	0.42	0.34
S_1	0.96	0.82	0.77	0.68	0.83	0.66	0.75	0.47
S_2	**1.00**	0.92	**0.91**	0.78	0.92	0.77	**0.91**	0.78
S_3	**1.00**	**0.98**	0.90	**0.82**	0.93	**0.83**	0.90	**0.80**
S_4	0.75	0.67	0.49	0.32	0.48	0.34	0.26	0.23
S_5	**1.00**	0.94	0.89	0.80	**0.96**	0.81	0.85	0.77

values (0.75, 0.55 and 0.78) were obtained by the geometrical feature G_4, while in the fourth set the geometrical feature G_3 yielded the best $AUC_{0.1}$ value (0.43). With respect to $AUC_{0.1}$ the best statistical feature was S_3 which yielded values of 0.98, 0.82, 0.83 and 0.80 on the four tablet types, respectively.

The ROC curves of individual geometrical and statistical features obtained on the first tablet type are shown in figure 8. The ROC curves further indicate that, among the geometrical features, G_4 performed the best and G_1 the worst, while among the statistical features, S_3 was the best and S_4 the worst. Among all features S_3 performed almost perfectly and was thus the best while G_1 was the worst.

The overall performances of individual features were assessed by the AUC_1 values. In figure 9 AUC_1 values for all defect categories ($D_{1–5}$) are given for individual features and tablet image sets. On the first and second image sets features S_2, S_3 and S_5 performed the best as they yielded AUC_1 values of 0.99 and 0.97, respectively. On the third image set, the best features were S_3 and S_5 with the AUC_1 value of 0.98, while on the fourth set the best AUC_1 values of 0.96 were obtained by features S_2 and S_3. Figure 9 also shows that on all four tablet types the statistical features, except feature S_4, had higher mean AUC_1 values and much more consistent performance, i.e. a smaller min–max range, than the geometrical features.

An example of a tablet with a relatively large defect (D_4–deboss) is shown in figure 10. The first row shows original tablet image intensities (**I**), corresponding geometrical (Ω_1 and Ω_2) representations and statistical representations of intensities ($\tilde{\mathbf{I}}$), absolute gradients ($\tilde{\mathbf{G}}$) and gradients ($\tilde{\mathbf{C}}$). The second and third rows show images of feature values at each image point

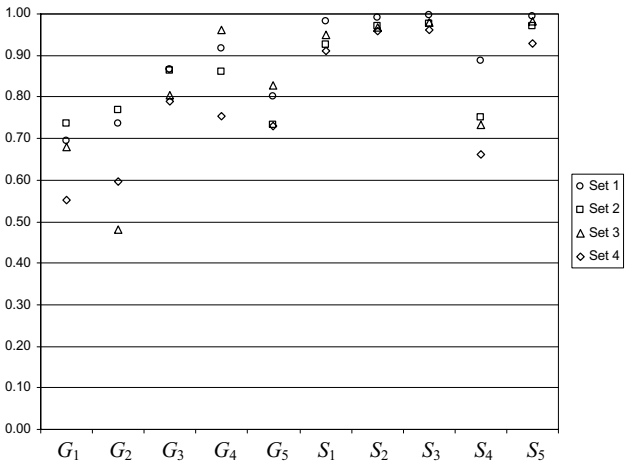

Figure 9. AUC_1 values of all geometrical (G_1–G_5) and all statistical (S_1–S_5) features on the four tablet types.

from which geometrical (G_1–G_5) and statistical features (S_1–S_5) are respectively derived as maximal values.

Table 3 shows the results for the joined geometrical ($G_{1–5}$) and statistical ($S_{1–5}$) features. The results for all four tablet types are given by the areas AUC_{FPR} under the ROC curves for FPR values of 0.1, 0.2, 0.5 and 1, while in figure 11 the corresponding ROC curves are depicted only for the first tablet image set. The comparison of $AUC_{0.1}$ values in table 2 and $AUC_{0.1}$ values in table 3 reveals that linear defect classification by the joined five geometrical ($G_{1–5}$) or statistical

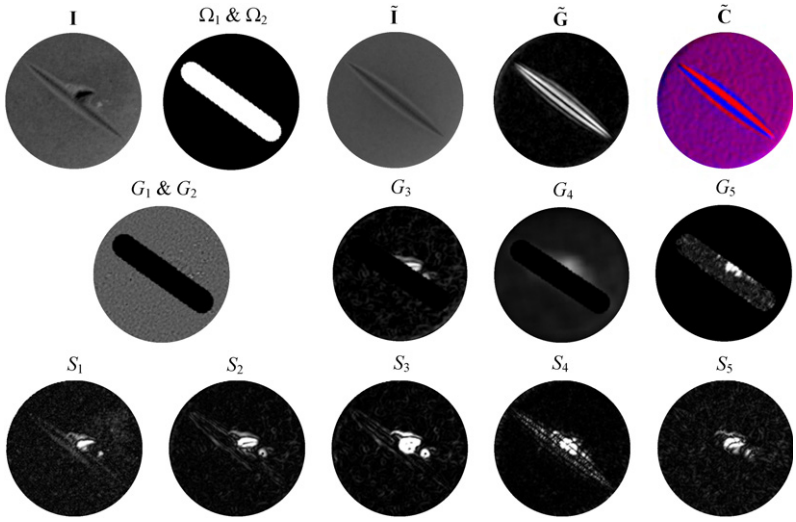

Figure 10. Image of defective tablet (**I**), geometrical (Ω_1 and Ω_2) and statistical ($\tilde{\mathbf{I}}$, $\tilde{\mathbf{G}}$ and $\tilde{\mathbf{C}}$) representations (top row) and the corresponding geometrical (G_1–G_5, middle row) and statistical features (S_1–S_5, bottom row).
(This figure is in colour only in the electronic version)

Table 3. $AUC_{0.1}$, $AUC_{0.2}$, $AUC_{0.5}$ and AUC_1 values for linear defect classification by the joined geometrical features ($G_{1–5}$) and statistical features ($S_{1–5}$) on all four sets of tablet images.

	$AUC_{0.1}$		$AUC_{0.2}$		$AUC_{0.5}$		AUC_1	
Set	$G_{1–5}$	$S_{1–5}$	$G_{1–5}$	$S_{1–5}$	$G_{1–5}$	$S_{1–5}$	$G_{1–5}$	$S_{1–5}$
1	0.96	0.99	0.98	0.99	0.99	1.00	1.00	1.00
2	0.72	0.84	0.75	0.89	0.83	0.96	0.91	0.98
3	0.85	0.88	0.93	0.94	0.97	0.98	0.99	0.99
4	0.66	0.86	0.78	0.90	0.89	0.95	0.95	0.97

Table 4. The $AUC_{0.1}$ values for individual (S_1–S_5) and joined ($S_{1–5}$) statistical features of tablets in the first set, given as a function of the number of PCA components.

	Number of PCA components					
Feature	0	1	2	3	4	5
S_1	0.73	0.75	0.77	0.82	0.81	0.82
S_2	0.78	0.89	0.90	0.92	0.94	0.96
S_3	**0.90**	**0.96**	**0.97**	**0.98**	**0.98**	**0.99**
S_4	0.68	0.63	0.66	0.67	0.67	0.67
S_5	0.78	0.89	0.94	0.94	0.96	0.96
$S_{1–5}$	**0.97**	**0.99**	**0.99**	**0.99**	**1.00**	**1.00**

($S_{1–5}$) features yields significantly better defect detection than by individual (G_1–G_5) or (S_1–S_5) features.

Table 4 shows the defect detection performance ($AUC_{0.1}$ values) as a function of the number of PCA components used in statistical models. The results are given for the first set of tablets, all defect categories ($D_{1–5}$), and for each individual (S_1–S_5) and joined ($S_{1–5}$) statistical features. The features S_2, S_3 and S_5 show the best performance, regardless of the number of PCA components used, among which the S_3 feature yielded the highest $AUC_{0.1}$ values. The results of this sensitivity analysis show that the number of PCA components slightly affects the defect detection performance, which was to be expected. However, the differences in the performances were larger for individual features, while the performances of the joint features were rather independent of the number of PCA components, except for the mean tablet representation (0 PCA components) that yielded slightly lower performance.

4. Discussion

Two alternative image analysis methods, based on geometrical and statistical *a priori* knowledge, were introduced and compared for visual inspection of typical production defects on imprinted tablets. The contribution of this work to the field of automated visual inspection of tablets is threefold. First, a novel imprint specific geometrical feature in the form of a gradient component in the direction of the imprint was proposed. Next, a set of statistical features, estimating the discrepancy between the analysed image and the statistical *a priori* knowledge on the appearance of the whole tablet, was first proposed for automated visual inspection of tablets. Last, but not least, the systematic evaluation methodology for assessing the sensitivities and specificities for detecting various defects on tablets by the ROC analysis was suggested for objectively assessing the performances of the existing and emerging tablet inspection systems.

The geometrical and statistical methods were tested on a large representative image database of four types of tablets. The obtained results demonstrate that both methods perform adequately, although the statistical method yielded better sensitivity and specificity on all types of tablets and defects. The geometrical features G_1 and G_2 can be interpreted as a high pass filtering and are thus sensitive to small local bright and dark defects on tablet images, respectively. The features G_3 and G_4 estimate high intensity gradients on small and large scale, respectively. Feature G_5 is made sensitive to the intensity gradients in the local imprint direction and operates only on the imprint area. The image of G_5 feature values in figure 10 shows that imprint intensity gradients are highly suppressed by this imprint specific feature, while the gradients that are due to imprint defect are retained. Although

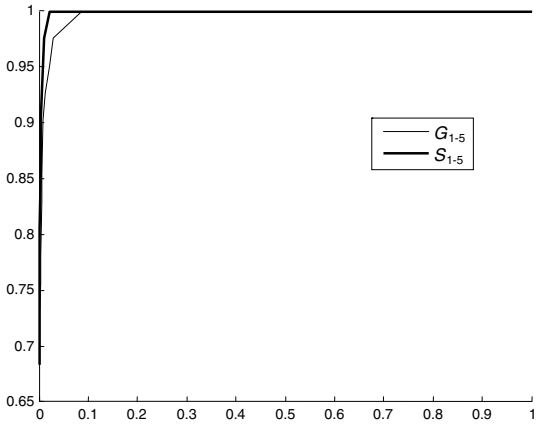

Figure 11. The ROC curves for defect detection by the joined geometrical ($G_{1–5}$, thin) and statistical ($S_{1–5}$, thick) features on the first set of tablets.

the features G_3 and G_4 showed the best sensitivity to all types of defects, none of the geometrical features can be considered as defect specific. Namely, all the features are more or less sensitive to large defects but for small and specific defects, the features proved to be complementary as the best defect detection results were obtained by the joined classification. Similar conclusions can be drawn for the statistical features, although these proved to be less complementary, likely because individual features themselves yielded good and comparable performance on various defects. Statistical features measure the difference between image representations, i.e. intensity, absolute gradient or gradient representation and their reconstructions by corresponding statistical models. The statistical features S_1 and S_2 estimate the differences between the intensities and absolute gradients, respectively. On the other hand, the features S_3, S_4 and S_5 estimate also the differences in the gradient orientations in the inspected image and its statistical representation. Like geometrical features, statistical features can also not be considered as defect specific. On the other hand, the sensitivity of geometrical and statistical features can be tuned to defects of different scales by changing the sizes of corresponding filters. The larger the filters, the higher the sensitivity to larger tablet surface defects. On the other hand, the smaller the filters the higher the sensitivity to small surface defects but also to image noise. However, the sensitivity to image noise can be efficiently suppressed by filtering original image intensities. In both methods, the features based on image gradients outperformed the features based on image intensities. Altogether, the statistical features based on component gradients performed the best, which was to be expected since component gradients are generally more descriptive than absolute gradients or intensities.

Even better defect detection was obtained by the joined geometrical or statistical features in a linear classification with boundaries parallel to the features axes. For the joined linear classification the statistical method performed slightly better than the geometrical one. The improvement of the joined over individual features was thus relatively higher for geometrical than for the statistical method. This indicates that individual geometrical features are more complementary than the statistical ones. Nevertheless, the improvement of the joined classification with the less complementary statistical features was still significant, which justifies the use of the joined feature defect classification.

From the practical point of view, the reliability and speed of the inspection and simplicity of the training required by both methods before inspecting a new type of product, are of utmost importance. The geometrical method requires the construction of a skeleton and corresponding binary model of an imprint, which can be obtained automatically from the tablet design or manually on a selected tablet image. On the other hand, the statistical method requires construction of statistical models of appearances that can be derived automatically from the aligned training images of each new tablet type. Therefore, considering the training phase, the statistical method may be more automated and thereby also more practical but requires reliable rigid registration of tablet images. Image registration also plays an important role in the inspection phase of both methods. Namely, the geometrical and statistical methods require automatic rigid registration of the inspected tablet image to the corresponding geometrical and statistical models, respectively. Fortunately, rigid registration is a well-established image analysis field [18]. The registration methods [11, 12] were evaluated by a dedicated 'gold standard' registration and proved to be fast (<4 ms), highly accurate (0.74°) and robust (99.8%). These highly accurate registration errors have no significant impact on defect detection performance, except for the large defects that cause the registration to fail completely. However, this has no practical implications as tablets with large defects have to be discarded anyway. Considering the inspection phase, i.e. the computation of tablet features, the obtained results indicated that the statistical method yields better reliability of defect detection. However, the computational load of the statistical method is higher as, besides the computation of features, this method additionally requires the approximation of tablet surface appearance. Since this additional step can be significantly accelerated [19], the statistical method is just slightly slower than the geometrical one and thereby feasible for real-time visual inspection of imprinted tablets. The proposed methods were implemented in C++ and tested on a PC with an Intel Pentium IV 3.2 GHz processor. Segmentation, registration and gradient computation in the first set of tablets took on average 0.4 ms, 3.9 ms and 0.3 ms, respectively. Geometrical feature computation in the first set of tablets took on average 0.4 ms, 0.2 ms, 0.5 ms and 0.1 ms respectively for $G_{1–2}$, G_3, G_4 and G_5 features. Statistical feature computation in the first set of tablets took on average 2.6 ms, 2.6 ms and 5.6 ms for S_1, S_2 and $S_{3–5}$ features, respectively. The approximate time needed for image pre-processing and computation of both geometrical and statistical features was 15 ms per tablet in the first set. Therefore, the inspection speeds of approximately 66 tablets per second, i.e. 240 000 tablets per hour, can be obtained even for the large tablets from the first set. Since the inspection speed depends mainly on the tablet size, smaller tablets could easily be inspected with the speed of 100 tablets per second, i.e. 360 000 tablets per hour, which is sufficient for the current pharmaceutical tablet production rates and outperforms all of the currently available tablet inspection machines.

5. Conclusion

The high specificity (low FPR) of the visual quality inspection has huge practical and economical benefits as fewer non-defective products are detected as defective and thereby mistakenly discarded. On the other hand, the increased sensitivity (high TPR) is of utmost importance for the final quality of a given tablet batch. In terms of specificity and sensitivity, the statistical defect detection method and especially the component gradient features seem feasible for visual quality inspection of different types of tablets. Nevertheless, both presented image analysis methods are quite general and promising tools for automated visual inspection of not only tablets but also capsules or other solid oral dosage forms. The methods are currently tested on large tablet batches in industrial environment and already indicate a high practical value. Our future efforts will be focused on further optimization of the training phase and code optimization with the aim of further increasing the flexibility and adaptability of the inspection machine to different products (such as capsules, chewing-gum, beans, coffee, etc) and reaching even higher inspection speeds.

Acknowledgments

This work was supported by the Ministry of Higher Education, Science and Technology, Republic of Slovenia under the grants P2-0232, L2-7381, L2-9758 and Z2-9366.

References

[1] Albion K, Briens L, Briens C and Berruti F 2006 Detection of the breakage of pharmaceutical tablets in pneumatic transport *Int. J. Pharm.* **322** 119–29

[2] FDA Code of Federal Regulations (21CFR206) Imprinting of solid oral dosage form drug products for human use, available at http://www.accessdata.fda.gov/scripts/cdrh/cfdocs/cfcfr/CFRSearch.cfm?CFRPart=206

[3] Berman A 2004 Reducing medication errors through naming, labeling, and packaging *J. Med. Syst.* **28** 9–29

[4] Newman T S and Jain A K 1995 A survey of automated visual inspection *Comput. Vis. Image Underst.* **61** 231–62

[5] Malamas E N, Petrakis E G M, Zervakis M, Petit L and Legat J D 2003 A survey on industrial vision systems, applications and tools *Image Vis. Comput.* **21** 171–88

[6] Deutschl E and Rinnhofer A 1998 Tablet quality assurance in real time *Proc. 14th Int. Conf. on Pattern Recognition (Brisbane, Australia) IEEE Computer Society* **vol 2** pp 1731–4

[7] Silvennoinen R, Peiponen K E, Laakkonen P, Ketolainen J, Suihko E, Paronen P, Rasanen J and Matsuda K 1997 On the optical inspection of the surface quality of pharmaceutical tablets *Meas. Sci. Technol.* **8** 550–4

[8] Wagner K G, Krumme M and Schmidt P C 1999 Investigation of the pellet-distribution in single tablets via image analysis *Eur. J. Pharm. Biopharm.* **47** 79–85

[9] Peiponen K E, Silvennoinen R, Räsänen J, Matsuda K and Tanninen V P 1997 Optical coating inspection of pharmaceutical tablets by diffractive element *Meas. Sci. Technol.* **8** 815–8

[10] Derganc J, Likar B, Bernard R, Tomaževič D and Pernuš F 2003 Real-time automated visual inspection of color tablets in pharmaceutical blisters *Real-time Imaging* **9** 113–24

[11] Alpert N M, Bradshaw J F, Kennedy D and Correia J A 1990 The principal axes transformation—a method for image registration *J. Nucl. Med.* **31** 1717–22

[12] Jain A K 1989 *Fundamentals of Digital Image Processing* (Englewood Cliffs, NJ: Prentice-Hall) pp 434–8

[13] Cootes T F, Edwards G J and Taylor C J 2001 Active appearance models *IEEE Trans. Pattern Anal. Mach. Intell.* **23** 681–5

[14] Moghaddam B and Pentland A 2000 *Probabilistic, View-Based, and Modular Models for Human Face Recognition* (New York: Academic) pp 837–52

[15] Press W H, Teukolsky S A, Vetterling W T and Flannery B P 1992 *Numerical Recipes in C: The Art of Scientific Computing* (Cambridge: Cambridge University Press) pp 59–70

[16] Sonka M, Hlavac V and Boyle R 1999 *Image Processing, Analysis and Machine Vision* 2nd edn (The University of Iowa: Brooks/Cole) pp 79–80

[17] Fawcett T 2006 An introduction to ROC analysis *Pattern Recognit. Lett.* **27** 861–74

[18] Zitova B and Flusser J 2003 Image registration methods: a survey *Image Vis. Comput.* **21** 977–1000

[19] Leonardis A and Bischof H 2000 Robust recognition using eigenimages *Comput. Vis. Image Understand.* **78** 99–118